NREL/TP-451-5737 • UC Category: 271 • DE93018205

Microscopic Origins of Metastable Effects in a-Si:H and Deep Defect Characterization in a-Si,Ge:H Alloys

Annual Subcontract Report
1 February 1992 – 31 January 1993

RECEIVED
SEP 02 1993
OSTI

J. David Cohen
University of Oregon
Eugene, Oregon

NREL technical monitor: B. von Roedern

National Renewable Energy Laboratory
1617 Cole Boulevard
Golden, Colorado 80401-3393
Operated by Midwest Research Institute
for the U.S. Department of Energy
under Contract No. DE-AC02-83CH10093

MASTER

Prepared under Subcontract No. XG-1-10063-1

August 1993

DISTRIBUTION OF THIS DOCUMENT IS UNLIMITED

This publication was reproduced from the best available camera-ready copy submitted by the subcontractor and received no editorial review at NREL.

NOTICE

NOTICE: This report was prepared as an account of work sponsored by an agency of the United States government. Neither the United States government nor any agency thereof, nor any of their employees, makes any warranty, express or implied, or assumes any legal liability or responsibility for the accuracy, completeness, or usefulness of any information, apparatus, product, or process disclosed, or represents that its use would not infringe privately owned rights. Reference herein to any specific commercial product, process, or service by trade name, trademark, manufacturer, or otherwise does not necessarily constitute or imply its endorsement, recommendation, or favoring by the United States government or any agency thereof. The views and opinions of authors expressed herein do not necessarily state or reflect those of the United States government or any agency thereof.

Printed in the United States of America
Available from:
National Technical Information Service
U.S. Department of Commerce
5285 Port Royal Road
Springfield, VA 22161

Price: Microfiche A01
Printed Copy A03

Codes are used for pricing all publications. The code is determined by the number of pages in the publication. Information pertaining to the pricing codes can be found in the current issue of the following publications which are generally available in most libraries: *Energy Research Abstracts (ERA); Government Reports Announcements and Index (GRA and I); Scientific and Technical Abstract Reports (STAR)*; and publication NTIS-PR-360 available from NTIS at the above address.

Printed on recycled paper

DISCLAIMER

Portions of this document may be illegible electronic image products. Images are produced from the best available original document.

PREFACE

This Annual Technical Progress Report covers the work performed at the University of Oregon for the period 1 February 1992 to 31 January 1993 under NREL Subcontract Number XG-1-10063-1. The following personnel participated in this research program:

NAME	TITLE	WORK PERFORMED
J. David Cohen	Principal Investigator	Program Manager
John Hautala	Research Associate	ESR Measurements, a-Si:H Stability Studies
Thomas Unold	Research Assistant	Capacitance Characterization of a-Si,Ge:H Alloys
Fan Zhong	Research Assistant (4th Quarter Only)	Modulated Photocurrent Studies of a-Si,Ge:H Alloys

TABLE OF CONTENTS

Page

LIST OF ILLUSTRATIONS iii

LIST OF TABLES iii

EXECUTIVE SUMMARY iv

1.0 INTRODUCTION 1

2.0 SAMPLES

2.1 SAMPLE GROWTH 2
2.2 SAMPLE PREPARATION 3

3.0 EXPERIMENTAL METHODS

3.1 ADMITTANCE SPECTROSCOPY 3
3.2 DRIVE-LEVEL CAPACITANCE PROFILING 4
3.3 TRANSIENT PHOTOCAPACITANCE AND PHOTOCURRENT 5
3.4 ELECTRON SPIN RESONANCE 6

4.0 BASIC ASPECTS OF MOBILITY GAP STRUCTURE

4.1 OPTICAL GAPS AND URBACH SLOPES 7
4.2 MIDGAP DEFECT DENSITIES 9

5.0 DETAILED PROPERTIES OF DEEP DEFECTS AND TRANSPORT

5.1 DEFECT BAND OPTICAL TRANSITION ENERGIES 12
5.2 TRANSPORT 15

6.0 LIGHT INDUCED DEGRADATION STUDIES

6.1 OPTICAL EXPOSURE PROCEDURE 17
6.2 EXPERIMENTAL RESULTS 17

7.0 SUMMARY AND CONCLUSIONS 20

8.0 REFERENCES 22

LIST OF ILLUSTRATIONS

Page

FIG. 1. Germanium fraction in our alloy films as a function of the $GeH_4/(SiH_4+GeH_4)$ source gas ratios 2

FIG. 2. Comparison of the density of defects as determined by drive-level capacitance profiling and ESR for an intrinsic a-Si:H sample 6

FIG. 3. Transient photocurrent spectra for a series of five a-$Si_{1-x}Ge_x$:H films with different Ge fractions 8

FIG. 4. Variation of the optical gaps with the Ge fraction in our alloy films. 8

FIG. 5. Variation of Urbach bandtail energies, E_U, with alloy composition and with optical gap energies 10

FIG. 6. Drive-level determined deep defect densities *vs.* the alloy composition . . .11

FIG. 7. Comparison of transient photocapacitance and junction photocurrent spectra for an a-$Si_{1-x}Ge_x$:H sample (x = 0.47) at two temperatures. 13

FIG. 8. Schematic of optical transitions and thermal transitions incorporated in the modeling of the photocapacitance and photocurrent spectra 13

FIG. 9. Energy positions of the two defect bands inferred by the modeling of the photocapacitance and photocurrent spectra 14

FIG. 10. Dependence of the hole $\mu\tau$ products on alloy composition and also $(\mu\tau)_h N_D$ on alloy composition 16

FIG. 11. Transient photocurrent and photocapacitance spectra for the dark annealed and a light soaked state of an x = 0.29 a-$Si_{1-x}Ge_x$:H sample 18

FIG. 12. Hole $\mu\tau$ products *vs.* alloy composition before and after light soaking and the variation of $(\mu\tau)_h N_D$ before and after light soaking 19

LIST OF TABLES

TABLE I. Summary of Properties Determined for Photo-CVD a-$Si_{1-x}Ge_x$:H Series. .20

EXECUTIVE SUMMARY

Our research during Phase II of NREL Subcontract XG-1-10063-1 concentrated upon the evaluation of low mobility gap a-Si,Ge:H alloy films. A series of 8 a-Si,Ge:H alloy samples were grown by the photo-CVD method at the Institute for Energy Conversion, University of Delaware. The samples studied encompassed the range of optical gaps: 1.3 to 1.6 eV, and corresponding Ge fractions: about 20at.% to 60at.%. We employed a variety junction capacitance techniques to determine deep defect energies and densities, Urbach bandtail energies, and $\mu\tau$ products for holes. Electron microprobe analysis (performed at NREL) provided fairly accurate Ge fractions for our samples. Thus we have been able to establish clear trends in the measured electronic properties as a function of the Ge fraction. For a few samples we also have preliminary results on the changes in electronic properties caused by light induced degradation.

We conclude that these photo-CVD samples exhibit equal or superior properties in terms of bandtail widths and stable defect densities compared to any reported results on a-Si,Ge:H samples grown by glow discharge. Second, by assigning defect energy levels from a detailed analysis of our transient sub-band-gap photocapacitance and photocurrent spectra, we find clear evidence for *two* distinct defect sub-bands, one at roughly midgap and the other in the upper half of the gap. The midgap defect band is found to be correlated in its magnitude with companion ESR measurements of the densities of Ge dangling bonds in a couple samples. The shallow level, still of unknown origin, appears to exhibit a suppression of its thermal release of trapped electrons, suggesting significant lattice relaxation. Finally, we have found that the trapping lifetime related $\mu\tau$ products for holes decrease in direct proportion to the density of midgap defects in these samples. This appears to be the case regardless of whether we are dealing with stable defects or defects created by light soaking.

1.0 INTRODUCTION

The work carried out in Phase II under NREL Subcontract XG-1-10063-1 has again concentrated upon the evaluation of low mobility gap a-Si,Ge:H alloy films. Some additional work has been carried out to assess the effects of carbon impurities on the stability of a-Si:H film; however, these studies are still incomplete and thus will be presented in a later report. Also we have just begun a series of evaluations of the a-Si,Ge:H using modulated photocurrent techniques. These will also be reported later.

The experimental results described in this report are based primarily on a variety of junction capacitance techniques: admittance spectroscopy, transient photocapacitance (and photocurrent), and drive-level capacitance profiling. We were able to obtain a fairly extensive series of a-Si,Ge:H alloy samples grown by the photo-CVD method through a collaboration with researchers at the Institute for Energy Conversion, University of Delaware. This series of samples covers a range of optical gaps (1.3 to 1.6 eV) and corresponding Ge fractions (from about 20at.% to 60at.%).

We have continued the kinds of characterization reported last year for the first couple of these alloy samples. We have thus now determined deep defect energies and densities, Urbach bandtail energies, and $\mu\tau$ products for holes for the entire series. Using an updated analysis of the actual atomic compositions of our samples, the trends in the measured electronic properties with Ge fraction have become quite clear. In a few samples we also investigated the changes in electronic properties caused by light induced degradation, but results for this part of the study must still be considered preliminary. Nonetheless, we believe that our results clearly establish the fact that these photo-CVD a-Si,Ge:H alloy samples are among the best low gap material currently available. Thus the results reported here should provide a very useful baseline of film properties against which to compare samples produced by other methods.

In the Sections that follow, we first describe the samples studied and then briefly review the experimental techniques employed. In Section 4 we discuss our results concerning the basic electronic properties: optical gaps, Urbach energies, and overall defect densities. In Section 5 we present a more detailed analysis of the defect structure and also what we have learned of the transport properties from our measurements. In Section 6 we present our preliminary results on light induced effects in these samples. Finally, in Section 7 we summarize our findings and draw some general detailed conclusions.

2.0 SAMPLES

2.1 SAMPLE GROWTH

All of the samples utilized in this study were produced by the photo-CVD method by our collaborators at the Institute for Energy Conversion (C. Fortmann and Wayne Buchanen) at Delaware. In this method SiH_4/GeH_4 gas mixtures are subjected to UV radiation which excites a small added component of Hg in the gas mixture. These Hg atoms collide with the reactants to produce SiH_n and GeH_n radicals which then adhere to the substrate to produce the a-$Si_{1-x}Ge_x$:H film. Our series of 8 alloy samples were grown on p^+ crystalline Si substrates using SiH_4/GeH_4 gas ratios which varied between 3% to 15%. In addition, 2 photo-CVD samples at the endpoints (a-Si:H and a-Ge:H) were also examined.

The substrate temperature for all samples was 230°C and the reactor pressure was 5 torr. Total gas flows were typically 70sccm. Growth times of up to 7 hours were required to obtain films of the desired thickness (of at least 0.8μm). Further details of this growth method have been given elsewhere. [1]

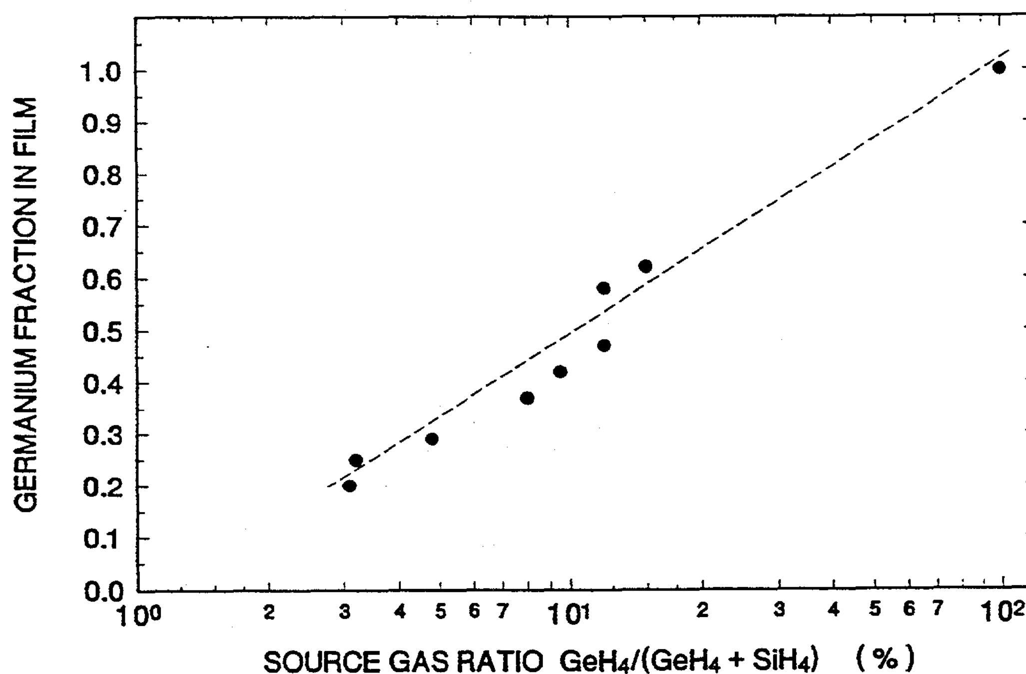

FIG. 1. Germanium fraction in our alloy films as a function of the $GeH_4/(SiH_4+GeH_4)$ source gas ratios employed for photo-CVD film growth. The Ge fractions were determined by electron microprobe measurements carried out at NREL. The SiH_4+GeH_4 source gases were further diluted with H_2.

The germanium fraction, x, for each of the alloy samples was determined using electron microprobe measurements with a 5 keV beam energy. These measurements were carried out courtesy of Harv Mahan and Alice Mason at NREL. In Fig. 1 we plot the actual Ge fraction in each film *vs.* the source gas SiH_4/GeH_4 ratios. This graph indicates a roughly logarithmic dependence of Ge content on the gas ratio. Thus we have determined that our series of 8 alloy films encompasses a composition range between 20at.% to 62at.%.

2.2 SAMPLE PREPARATION

We deposited a 0.5mm diameter (area = 2×10^{-3} cm^2) semitransparent Pd contact on the top surface of each sample. After annealing the sample with the contact for about 30min at 200°C, a $PdSi_2$ Schottky barrier is formed. Our test devices thus consist of a p^+ buried junction at the c-Si substrate in series with the Pd Schottky at the film surface. Each sample was mounted on a transistor header using In-Ga eutectic on the back of the substrate to make an ohmic contact to the c-Si.

3.0 EXPERIMENTAL METHODS

The measurements employed in our studies rely on a small set of experimental techniques which have all been described previously in some detail. They consist of (1) admittance spectroscopy as a function of temperature and frequency, (2) drive-level capacitance profiling, (3) transient photocapacitance taken together with transient junction photocurrent spectroscopy, and (4) electron spin resonance (ESR) spectroscopy. For the purpose of this report we will describe each method only very briefly and review what kind of information is obtained from each type of measurement.

3.1 ADMITTANCE SPECTROSCOPY

Our Schottky diode samples contain a depletion region which is characterized as a function of temperature and frequency before we undertake the more sophisticated capacitance based measurements described in Sections 3.2 and 3.3 below. Such measurements provide us with an estimate of our film thickness (the temperature independent region at low T is simply related to the geometric thickness, d, by the formula $C = \varepsilon A/d$), and an Arrhenius plot of the frequency of the lowest temperature capacitance step (or conductance peak) *vs.* $1/T$ provides us with the activation energy

of the ac conductivity, E_σ, which we identify with the Fermi energy position: $E_\sigma = E_C - E_F$. These admittance measurements also give us an indication of the quality of our Schottky barriers which allow us to pre-screen our samples for further study.

3.2 DRIVE-LEVEL CAPACITANCE PROFILING

The drive-level capacitance profiling method has been described in detail in many publications [2,3]. It is similar to other kinds of capacitance profiling in that it provides us with a density vs. distance profile; however, this particular method was developed specifically to address the difficulties encountered in interpreting capacitance measurements in amorphous semiconductors. In this method we monitor the junction capacitance both as a function of DC bias, V_B, and as a function of the amplitude of the alternating exciting voltage, δV. One finds that to lowest order this dependence obeys an equation of the form:

$$C(V_B, \delta V) = C_o(V_B) + C_1(V_B)\,\delta V + \ldots$$

and that the ratio

$$N_{DL} \equiv \frac{C_o^3}{2q_e\,\varepsilon A^2\,C_1}$$

is directly related to an integral over the density of mobility gap defect states:

$$N_{DL} \cong \int_{E_C-E_e}^{E_C-E_F^o} g(E)\,dE \quad .$$

Here E_F^o is the bulk Fermi level position in the sample and E_e depends on the frequency and temperature of measurement:

$$E_e(\omega,T) = k_B T \log(\nu/\omega)$$

Thus, by altering the measurment temperature (or frequency) we obtain information about the energy distribution of the defects and, by altering the applied DC bias, we can vary the spatial region at which we detect the defects in the sample. That is, we can spatially profile the defects as a function of the position from the barrier interface.

In our current studies we measured 100Hz profiles for a series of temperatures between 320K to 360K. These data usually indicated a clear upper limit for N_{DL} which, we have shown, is equal to roughly one half the total defect density in these samples

(see Section 3.4 below). This thus provides us with a quantitative measurment of the deep defect levels in these samples. In addition, because of the profiling information also obtained, we are able to assess the spatial uniformity of the electronic properties in these samples.

3.3 TRANSIENT PHOTOCAPACITANCE AND PHOTOCURRENT

The methods of junction transient photocapacitance and photocurrent have been discussed by us in great detail recently in the literature [4,5,6] and also in last year's NREL Annual Report. They represent types of sub-band-gap optical spectroscopy and provide spectra quite similar in appearance to PDS derived sub-band-gap optical absorption spectra or to CPM spectra. Instead of detecting absorbed energy, however, our photocapacitance and photocurrent transient methods detect the optically induced change in defect charge within the depletion region. However, unlike the CPM method, both of our junction based techniqes are not greatly influence by the free carrier mobilities since, once an electron (or hole) is optically excited into the conduction (valence) band it will either totally escape the depletion region on the slow timescale of our measurement (0.1 to 1s) or be retrapped into a deep state and not escape. In most cases we assume that almost all of the optically excited majority carriers (electrons) *do* escape but, in general, only a fraction of the minority carriers (holes).

Because the photocapacitance and photocurrent measurements have different sensitivities to the loss of electrons *vs.* holes from the depletion region, a detailed comparison of the two kinds of spectra can be used to disclose the escape length of the holes. This allows us to estimate the hole $\mu\tau$ products for these samples. In these experiments the parameter τ is identified as a deep trapping time, *not* a recombination time. We are also able to distinguish whether optical excitation of defect states comes about because of the excitation of trapped electrons to the conduction band or because of the excitation of valence band electrons into an empty mobility gap state. This ability to distinguish electron from hole processes is unique among all the various types of sub-band-gap optical spectroscopies. It is used to good advantage in Section 5.

(4) ELECTRON SPIN RESONANCE

Electron spin resonance (ESR) spectroscopy is generally used to determine the density of singly occupied deep defects. It provides an absolute density measurement, although it is insensitive to any population of charged defects. In the studies reported here this method has been employed only in a secondary mode to corroborate the defect densities determined by our drive-level profiling method. In this regard we have been able to establish quite good agreement, to within a factor of 2, between the two techniques. To illustrate this, in Fig. 2 we exhibit a direct comparison of the absolute defect densities determined by these two kinds of measurements for an intrinsic a-Si:H glow discharge sample in which we vary the metastable defect density through an extended series of light soaking exposures and, following this, by a series of partial anneals back to state A. [7] The agreement between the absolute defect densities found by the 2 methods is extremely good. Such comparisons have allowed us to utilize with considerable confidence our drive-level technique as the primary tool for estimates of deep defect densities.

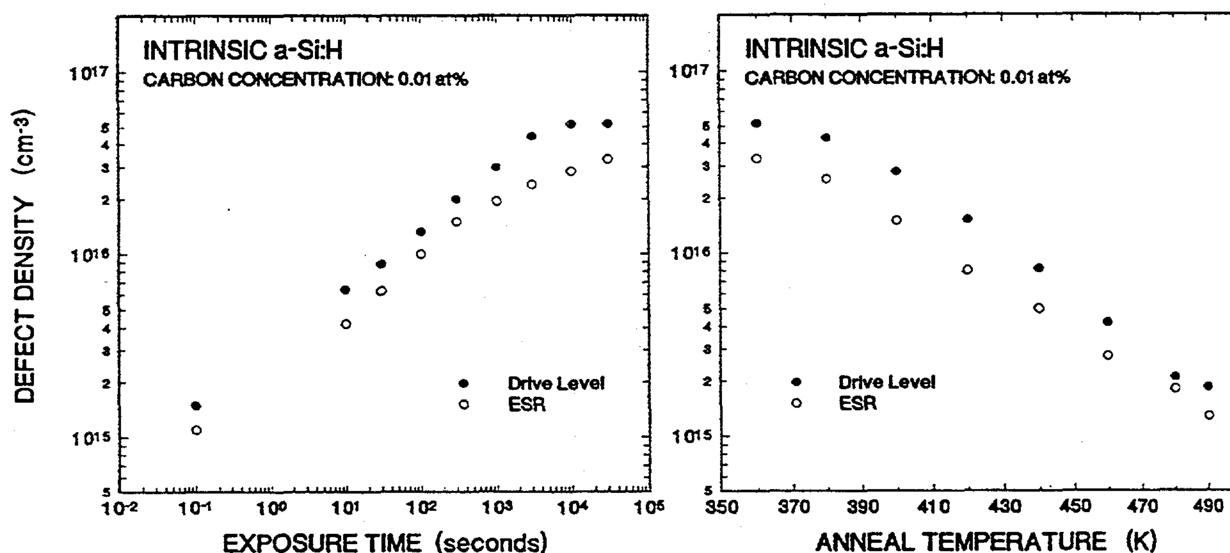

FIG. 2. Comparison of the density of defects as determined by drive-level capacitance profiling and ESR for an intrinsic a-Si:H sample. The defect density in this sample has been modified substantially through a sequence of light soaking steps and, following this, a series of partial anneals. The agreement between the absolute defect densities obtained by the two methods is seen to lie within a factor of two at each step within these series of metastable states.

4.0. BASIC ASPECTS OF MOBILITY GAP STRUCTURE

4.1 OPTICAL GAPS AND URBACH SLOPES

As discussed in Section 3.3, our transient photocurrent and photocapacitance methods provide a sensitive way to record the sub-band-gap optical transition spectra arising from mobility gap localized states. These methods have the advantage that they are much more sensitive than PDS optical absorption measurements, yet are superior to steady-state photoconductivity or CPM methods since the interpretation does not depend on the details of carrier transport.

A series of transient photocurrent spectra for 5 of our samples is shown in Fig. 3. [6] In this section we utilize such spectra to determine the Urbach slopes and optical gaps. We will temporarily restrict ourselves to results that can be obtained from a single spectrum type, and we will often rely more on the photocurrent measurements since they exhibit superior signal to noise. However, the determination of bandtail energies and optical gaps is quite consistent from either the photocapacitance or photocurrent spectra. A more detailed analysis based on both types of spectra together is discussed in Section 5.

In Fig. 3 we observe that the photocurrent spectra begin to flatten for the highest optical energies. This occurs for two reasons: first, that we begin to see the rollover from the exponential tail regime into the quadratic density of states of the valence band; and, second, because the exciting light becomes more strongly absorbed at higher optical energies and thus cannot excite carriers equally over the entire depletion region. Because these two competing effects occur within a similar energy regime, it is difficult to assign optical gaps to these samples from our spectra. Fortunately, for a few alloy compositions we also had at our disposal companion films on transparent substrates so that we could accurately determine the optical gaps. We then compared these transmission spectra with the corresponding transient photo-spectra so that we could establish an algorithm for finding the optical gaps directly from these latter measurements. The optical gaps determined in this fashion are plotted in Fig. 4 and correspond to E_{04} in each case. [8] For the samples where we also had transmission data, the value of the Tauc gap is also plotted and is generally found to be about 0.1eV smaller than E_{04}.

In Fig. 4 we clearly observe a linear reduction of the optical gap with increasing Ge content, x, which can be expressed in the form [8]

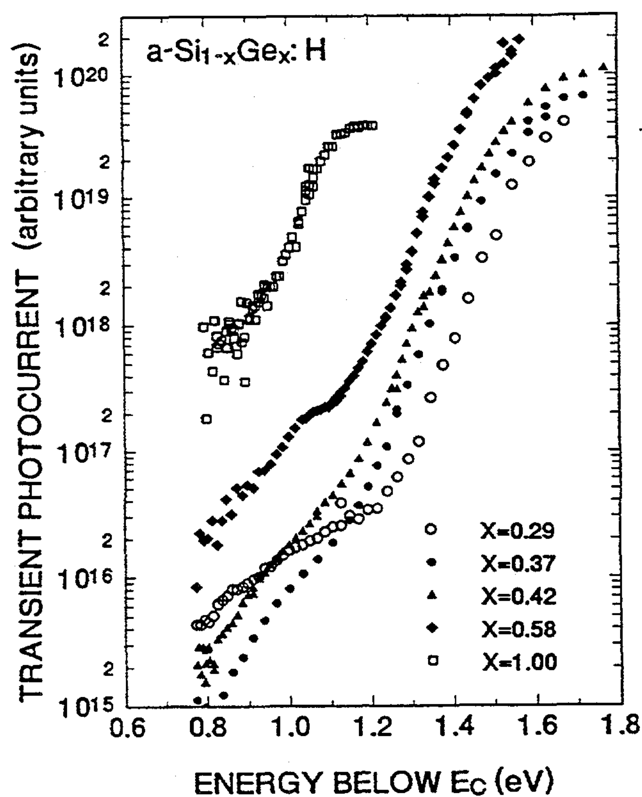

FIG. 3. Transient photocurrent spectra for a series of five a-$Si_{1-x}Ge_x$:H films with different Ge fractions as indicated.

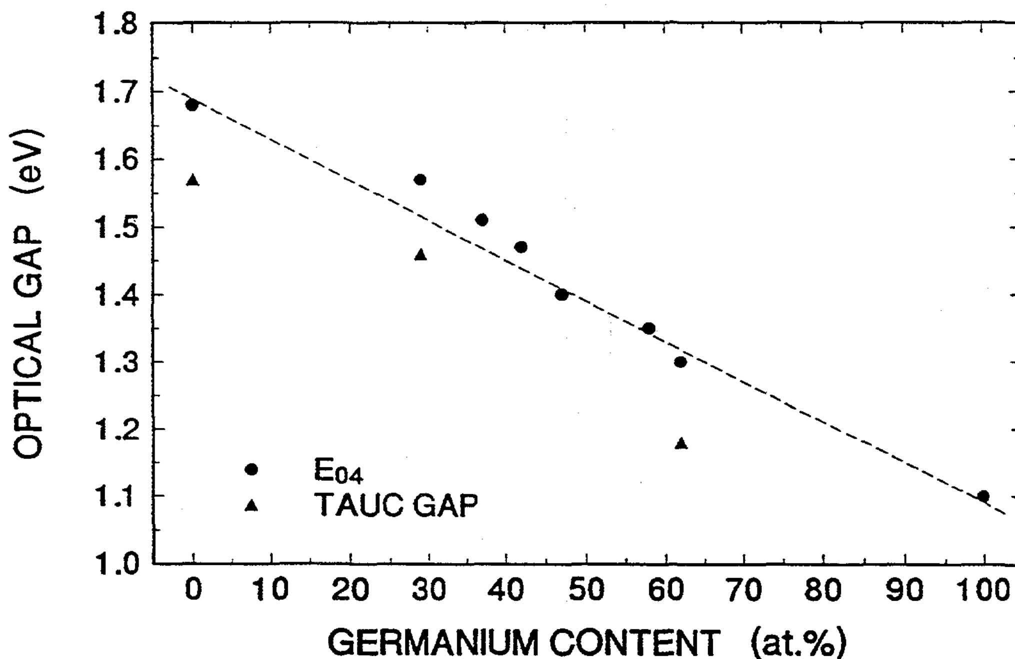

FIG. 4. Variation of the optical gaps, E_{04}, with the Ge fraction in our alloy films. For a few companion samples deposited on transparent substrates the value of the Tauc optical gap is also indicated.

$$E_{gap} = 1.7 \text{ eV} - (0.625 \text{ eV})\, x$$

This observed dependence agrees fairly closely with results obtained in studies of a-Si,Ge:H samples grown and characterized by other techniques [9,10].

Exponential Urbach tail regions are easily identified for all the spectra of Fig. 3. The spectral dependence on optical energy, hν, in this region, S(hν), obeys the functional form

$$S(h\nu) = S_0 \exp[(E_{gap} - h\nu)/E_U]$$

which defines the Urbach energy, E_U. The value of E_U obtained from our measurements is given in Fig. 5(a) as a function of Ge content and, in Fig. 5(b), as a function of optical gap. [8] In Fig. 5(b) we also show comparison data for samples grown by the glow discharge method as characterized by a couple other groups. We observe that the Urbach energies for the photo-CVD samples are roughly independent of alloy composition, lying in the range: $E_U = 52 \pm 4$ meV. This value of E_U is comparable to the best of the glow discharge samples produced by other groups.

4.2 MIDGAP DEFECT DENSITIES

The photocurrent spectra in Fig. 3 all exhibit a shoulder to the left of the exponential bandtail regime. This is due to the presence of deep defect bands. An analysis of the energies and location of these bands obtained by such spectra is given Section 5. A more direct and quantitative estimate of the total deep defect densities in these samples is obtained by the drive-level profiling measurements, as discussed in Section 3.2. In carrying out those measurements we determine a limiting upper value to N_{DL} by repeating such profiles at increasing temperatures. Then, assuming that this defect band lies near midgap, we infer that it is approximately 50% ionized in deep depletion. Thus, we double the upper limit value of N_{DL} to obtain our estimate of the total defect density. As discussed in Section 3.4 this estimate has been found to be quite consistent with values obtained from ESR measurements in a-Si:H samples.

Drive-level density estimates for 7 alloy samples plus one pure a-Si:H sample are plotted *vs.* Ge content in Fig. 6. [8] For two samples, reasonably accurate determinations of the defect density was also determined by ESR. These are plotted as open circles [7]. We see that the agreement between the two methods are quite good for the 30at.% Ge sample, but significantly different for the 62.at% Ge sample. This

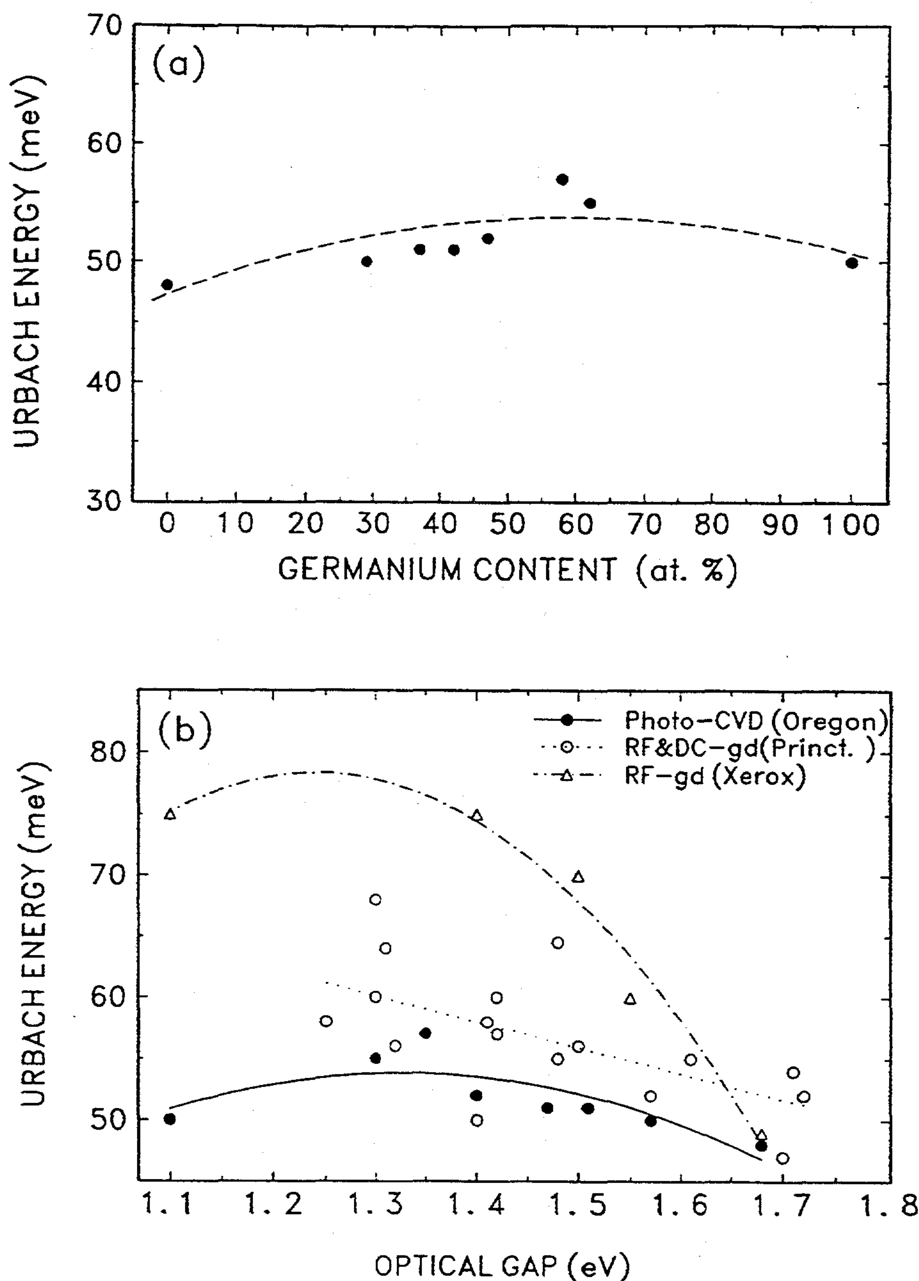

FIG. 5.(a). Variation of Urbach bandtail energies, E_U, with alloy composition. A relatively constant value of 52 ± 4 meV is indicated, roughly independent of Ge content. The dashed line is a guide to the eye which suggests that the endpoint films have somewhat narrower bandtails than the alloys in the middle of the composition range. (b) Comparison of E_U obtained for our photo-CVD samples with glow discharge samples of other groups as a function of the optical gap energy.

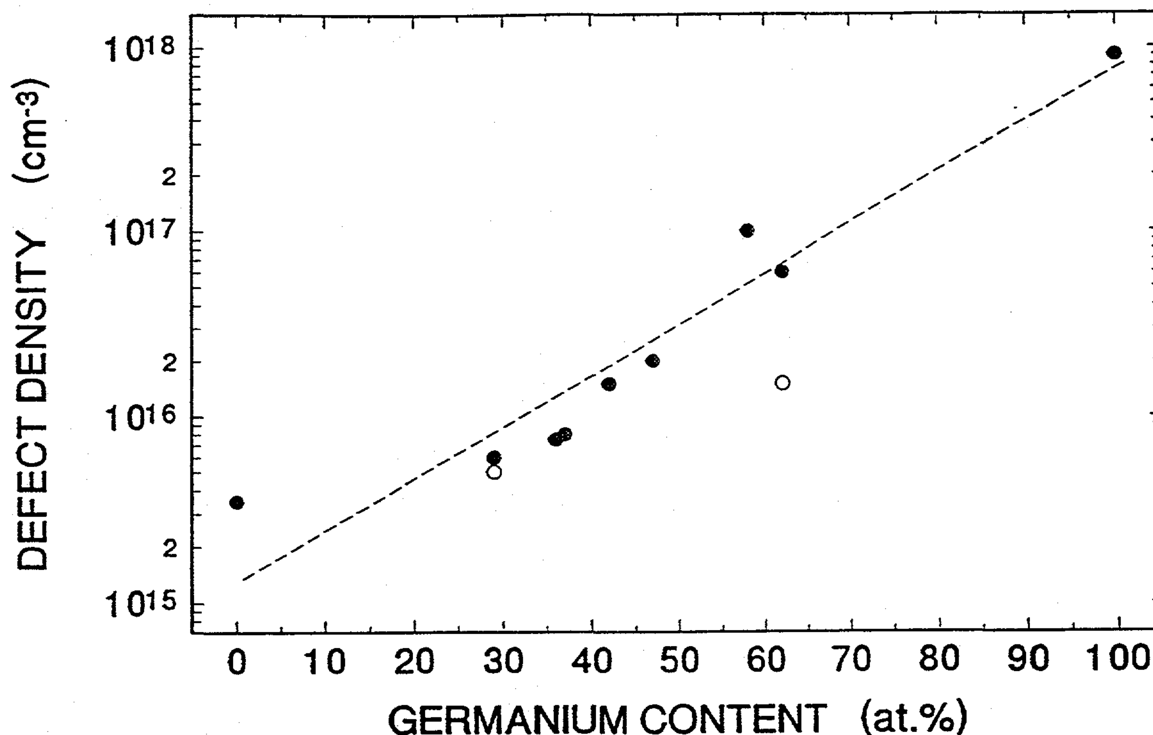

FIG. 6. Drive-level determined deep defect densities *vs*. the alloy composition. The dashed line indicates that the defect density increases exponentially with Ge content. The two data points plotted as open cirlces are the ESR determined defect densities for those samples.

suggests an increasingly important role for charged defects as the Ge fraction is increased. We also include a defect density estimate for a pure a-Ge:H sample from a detailed analysis of admittance *vs*. T measurements. (This sample was too thin to allow profiling measurements.) On this semi-logarithmic plot we obtain a reasonably good straight line fit for the variation of defect density with alloy composition. This implies an exponential increase in deep defect density with Ge content, such that we get a factor of 10 increase as the Ge fraction is increased from 20at.% to 60at.%. This range of compositions corresponds to a decrease in optical gap of 0.25eV (from 1.6 to 1.35eV). A very similar factor increase with decreasing optical gap has been reported by the Princeton group [9] for both D.C. and r.f. glow discharge alloy samples. They base their estimates on the integration of the defect band in CPM sub-band-gap absorption spectra. However, since they calibrate their absolute densities to values obtained using ESR, we can compare our results fairly directly. Thus we conclude that the absolute defect densities are at least a factor of two smaller for our photo-CVD samples than for their glow discharge samples.

5.0 DETAILED PROPERTIES OF DEEP DEFECTS AND TRANSPORT

5.1 DEFECT BAND OPTICAL TRANSITION ENERGIES

As discussed in detail in last year's Annual Report and in several of our published papers [4,5,6,11], important additional information can be obtained through a detailed comparison of the photocapacitance and photocurrent sub-band-gap spectra. In Fig. 7 we exhibit such pairs of spectra for two different measurement temperatures for one alloy sample. We see that the two types of spectra exhibit good qualitative agreement in general, and give nearly perfect quantitative agreement with respect to optical gap and Urbach bandtail energies. However, the details of the shape in the defect band regime differ significantly (optical energies below about 1.3 eV), and this is especially true at higher measurement temperatures.

The differences in the two kinds of spectra are attributed to the fact that hole currents *add* to any electron currents caused by the optically induced release of trapped carriers, but *subtract* from the resultant charge changes in the depletion region, as monitored by the photocapacitance technique. At lower temperatures hole motion is minimal (effective hole mobilities are small and so they are quickly retrapped); thus the observed differences are also small. At higher temperatures, however, the net motion of the holes increases and we therefore observe at larger difference between the spectra.

As discussed in last year's report and elsewhere [5,6,8], we can successfully model these differences by incorporating the set of optical transitions shown schematically in Fig. 8. This analysis has yielded the following general conclusions for all the alloy samples studied: (A) There exists a well defined set of defect transitions for a band located near midgap [transition (1) in Fig. 8]. It is this defect band which we believe to be connected with the defect densities determined by our drive-level profiling measurements. (B) There exists a second well defined defect band above midgap and also above the Fermi energy. This defect band gives rise to transitions from the valence band [transition (2')] with an accompanying motion of the residual valence band hole. However, we have determined that the subsequent thermal emission of the electron that was excited into the empty defect state is greatly suppressed, even at elevated temperatures. (C) There exist a combination of valence band or valence bandtail to conduction band or conduction bandtail transitions [transitions (2) and (3) plus others] which result in the Urbach exponential tail part of each spectrum. The magnitude of the photocapacitance spectrum is suppressed at

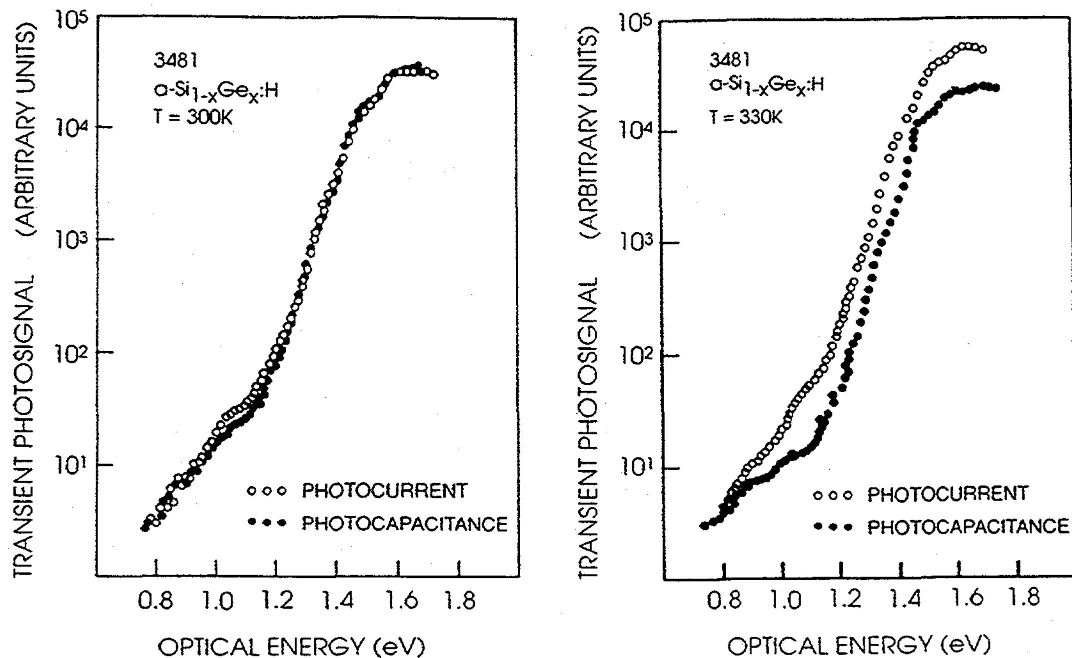

FIG. 7. Comparison of transient photocapacitance (solid circles) and junction photocurrent spectra (open circles) for an a-$Si_{1-x}Ge_x$:H sample ($x = 0.47$) at two temperatures as indicated. The capacitance measurement frequency was 1kHz and the transient measurement time window was 0.4 s. The two types of spectra have been overlapped in the lowest optical energy regime, and the differences observed between the higher temperature spectra indicate the existence of hole processes.

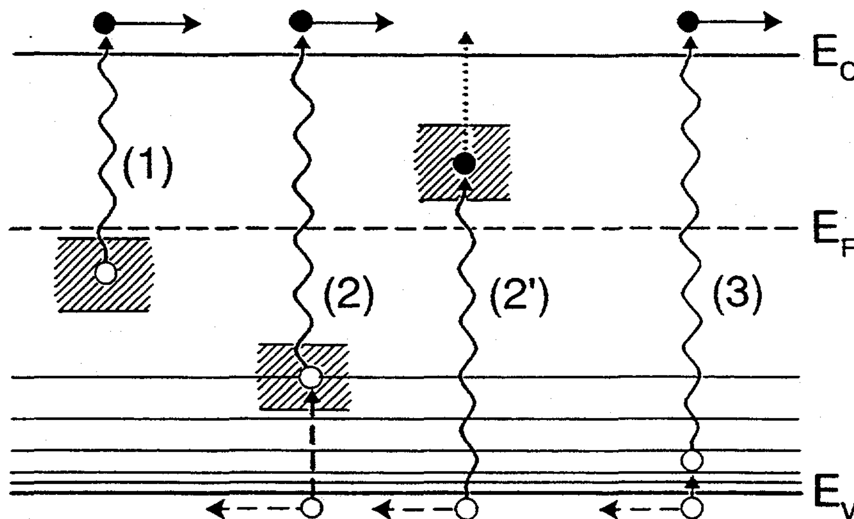

FIG. 8. Schematic of optical transitions (wavy lines) and thermal transitions (dashed lines) incorporated in the modeling of the a-$Si_{1-x}Ge_x$:H photocapacitance and photocurrent spectra obtained experimentally. The dotted line for the thermal transition step in process 2' indicates that electron emission for this process appears to be considerably suppressed.

higher temperature, however, due to resultant hole motion. Indeed, the ratio of the magnitudes of the photocapacitance and photocurrent signals in this energy regime (which is roughly constant) allows us to establish the deep trapping $\mu\tau$ products of these holes. The results of this part of the analysis is discussed in Section 5.2 below.

In Fig. 9 we plot the energy positions of the two defect bands mentioned above as a function of the Ge content in each sample. [8] The optical gap energies are also plotted for comparison. We observe that the midgap defect band tracks more closely conduction band edge than the valence band edge so that its nearly midgap position in pure a-Si:H tends to become slightly deeper than midgap as we move toward pure a-Ge:H. The second, shallower defect band also may be exhibiting the same general behavior, although the limited range of data makes this conclusion less certain at present.

As discussed in last year's report, the unusually large thermal release threshold for the shallower defect level suggests that electrons placed into this defect sub-band may undergo significant lattice relaxation. This conclusion is consistent with recent findings by the Tauc group [12] based upon photo-induced absorption studies of a-Si,Ge:H alloys. This unusual aspect of defect dynamics may have significant deleterious consequences on electron transport in the alloys, as has been discussed by other researchers [13,14]. We are presently unable to offer a plausible hypothesis concerning the origin of this defect band. However, we believe the deeper, midgap band is due to the Ge dangling bond. We base this upon the very good agreement between the defect densities obtained from drive-level profiling measurements and our ESR spin density determinations. In the latter case it is definite that we are dealing with Ge dangling bond defects.

FIG. 9. Energy positions (with respect to the valence band mobility edge) of the two defect bands inferred by the modeling of the photocapacitance and photocurrent spectra according to the transition processes shown in Fig. 9. The energy of the optical gap (E_{04}) for each of the films is also shown for reference.

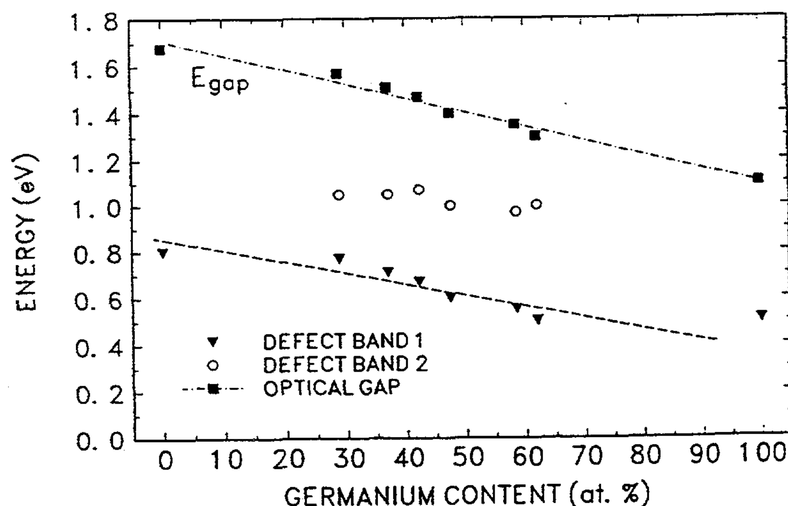

5.2 TRANSPORT

We mentioned above that the ratio of photocapacitance and photocurrent signals in the bandtail region is related the $\mu\tau$ products of the free holes. This is because optical excitation near the optical gap leads to the generation of free electrons and holes in roughly equal numbers. If both types of carriers were to escape the depletion region with equal probability, the net charge change, and hence the transient photocapacitance signal, would be nearly zero. However, the transient photocurrent signal would be enhanced. In general, then, the degree of suppression of hole escape will increase the relative ratio, R, of the photocurrent to the photocurrent signals, and this ratio can be used to determine the retrapping distance of the liberated hole, $(\mu\tau)_h$.

As presented in detail elsewhere [4,6,8], we have derived an explicit expression for $(\mu\tau)_h$ in terms of R and the charge density, N_+, in deep depletion of our sample. This latter quantity is obtained experimentally by our drive-level profiling measurements in the limit of increasing temperature (as discussed in Section 4.2). We obtain [15]

$$(\mu\tau)_h \quad = \quad \frac{\varepsilon}{q_e N_+} \log\left[(R+1)/2R\right]$$

We can illustrate the use of this formula for the data exhibited in Fig. 7(b). The two spectra have been aligned so that they overlap in the low optical energy regime. This alignment is based upon the assumption that only free electrons can be excited at the lowest optical energies so that both types of signals should give the same response ($R \equiv 1$). The ratio for optical energies above $h\nu = 1.3\text{eV}$ is then roughly constant at $R = 3.7$, and our drive level measurements give $N_+ = 1.5 \times 10^{16}\ \text{cm}^{-3}$. Hence we obtain $(\mu\tau)_h = 5 \times 10^{-10}\ \text{cm}^2/\text{V}$. Note that the value we obtain depends on the measurement temperature [that is, compare Figs. 7(a) and 7(b)] but reaches a limiting value as temperature is increased. It is this limiting value that we report. Indeed, our $(\mu\tau)_h$ evaluation is quite consistent with trapping time derived $(\mu\tau)_h$ products determined by other methods [9].

In a like manner we have determined $(\mu\tau)_h$ for most of our photo-CVD a-Si,Ge:H samples. The dependence of this quantity on Ge content, x, is displayed in Fig. 10(a). [8] We clearly observe a monotonic *decrease* in $(\mu\tau)_h$ as the Ge fraction is increased. Since the density of defects *increases* in this region, the observed decrease in $(\mu\tau)_h$ may simply reflect the increased likelihood of deep trapping due to the extra defects. Thus in

Fig. 10(b) we plot the product $(\mu\tau)_h N_D$ *vs.* x. Here we observe a fairly constant dependence except at the very largest Ge fraction. The observed marked decrease in $(\mu\tau)_h N_D$ for $x > 0.5$ is perhaps due to a larger hole capture cross-section which in turn could be due to an increased fraction of charged defects for the higher Ge containing alloys.

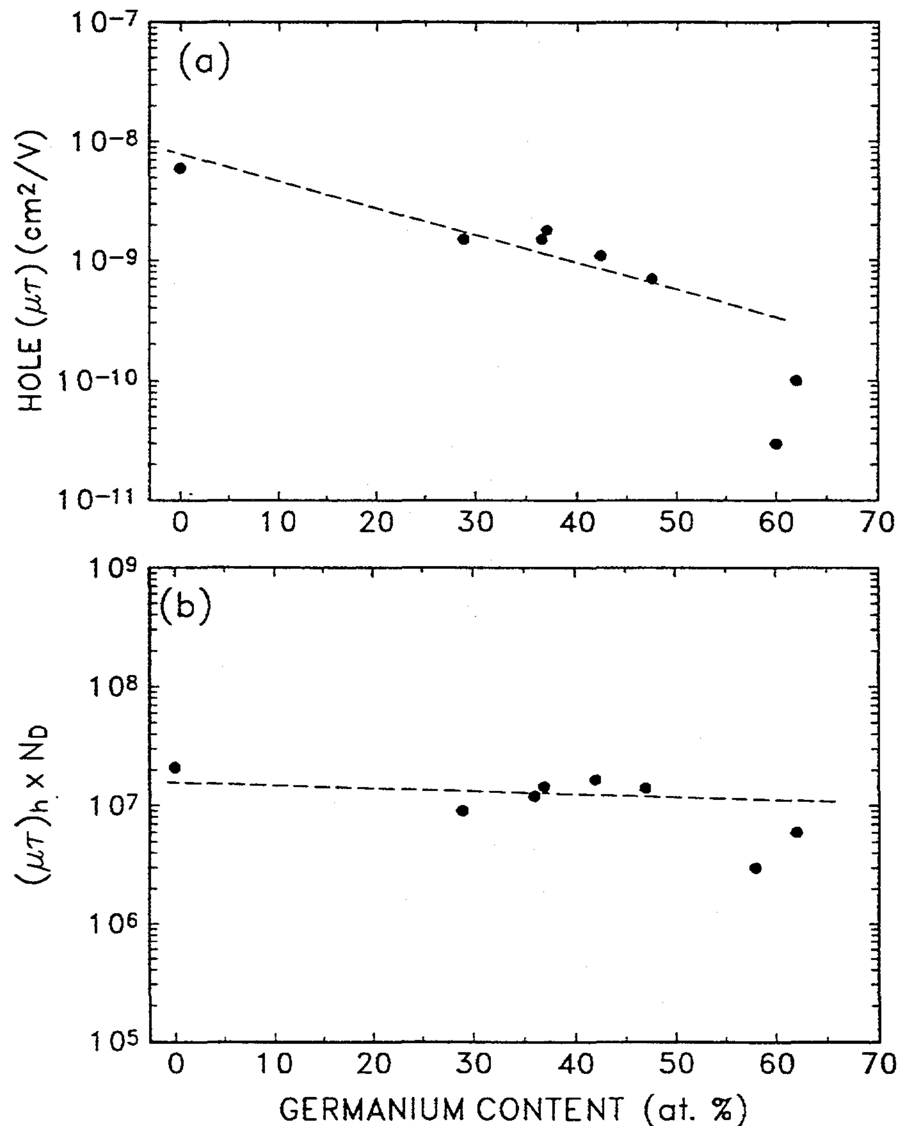

FIG. 10. (a). Dependence of the hole $\mu\tau$ products on alloy composition deduced from the analysis of the photocurrent/photocapacitance ratios in the bandtail region as explained in the text. (b) Variation of $(\mu\tau)_h$ multiplied by the corresponding defect densities [that is, $(\mu\tau)_h N_D$] on the alloy composition, indicating a more nearly constant dependence.

6.0 LIGHT INDUCED DEGRADATION STUDIES

6.1 OPTICAL EXPOSURE PROCEDURE

For the preliminary results of our light soaking studies reported in this section, we used a variety of light sources. For studies involving pure a-Si:H samples (including those discussed in Section 3.4) we used a Kr ion laser in the 650nm mode at an intensity of 4.5W/cm^2 ($G \approx 10^{22}\ \text{cm}^{-3}\text{s}^{-1}$). For most of our alloy samples we did not have access to a suitable laser source so that, instead, a ELH source was employed with suitable filters so we could obtain near optical gap light (this was necessary in ensure uniform absorption). This resulted in much lower exposure rates ($G < 10^{21}\ \text{cm}^{-3}\text{s}^{-1}$) so that was little chance of achieving saturation. For one alloy film, however, a Ti-sapphire laser tuned to 800nm was available so that a similar generation rate as for our a-Si:H sample ($10^{22}\ \text{cm}^{-3}\text{s}^{-1}$) could be utilized.

6.2 EXPERIMENTAL RESULTS

In Figure 11 we display photocapacitance and photocurrent spectra before and after light soaking for an alloy sample containing 29at.% Ge. [5] The light exposure in this case consisted of a 50 hour exposure at 400mW/cm^2 from a filtered ELH source. Both pairs of spectra in Fig. 11 were taken in the high temperature regime (350K) so that we could clearly observe the effects of any hole processes. For state A (the lower spectra with the square symbols) we observe a fair amount of splitting in the bandtail regime for the two kinds of spectra indicating a reasonable value of $(\mu\tau)_h$ of about $1.5 \times 10^{-9}\ \text{cm}^2/\text{V}$. After light soaking (the upper spectra with circle symbols) this splitting is substantially reduced which indicates a dramatic decrease in $(\mu\tau)_h$, to about $4 \times 10^{-10}\ \text{cm}^2/\text{V}$. In addition, we observe an almost factor of 3 increase in the defect band absorption (the feature near 1.0 eV). This has been made more evident by the dashed curve in Fig. 11(a) which is a re-plot of the state B photocurrent spectrum on top of the state A photocurrent spectrum so that they can be compared directly. A very similar factor increase (2.7) was also obtained by our drive-level evaluation of the deep defect densities.

Because of the very different light exposures employed it is quite difficult to compare the degree of light induced defect creation in the different samples at the present time. As explained in Section 6.1, we can be sure of reaching saturation only for the laser exposed samples: the pure a-Si:H and the 47at.% a-Si,Ge:H film. In Fig. 12(a),

we have nonetheless plotted the $(\mu\tau)_h$ products before and after light exposure for 4 alloy films plus those for a pure a-Si:H photo-CVD sample. [8] In spite of the uncertainties regarding the degree of saturation, we can definitely conclude that a significant degree of degradation in the hole transport is observed for all 4 of the alloy films. Furthermore, if we plot the quantity $(\mu\tau)_h N_D$ vs. x, as we did in Fig. 10(b) for the annealed samples, we discover a fairly constant dependence [see Fig. 12(b)]. This again indicates that the dominant cause of the limited $(\mu\tau)_h$ products determined in our measurements is simply the deep defect density itself, at least for alloy films with less than 50at.% Ge.

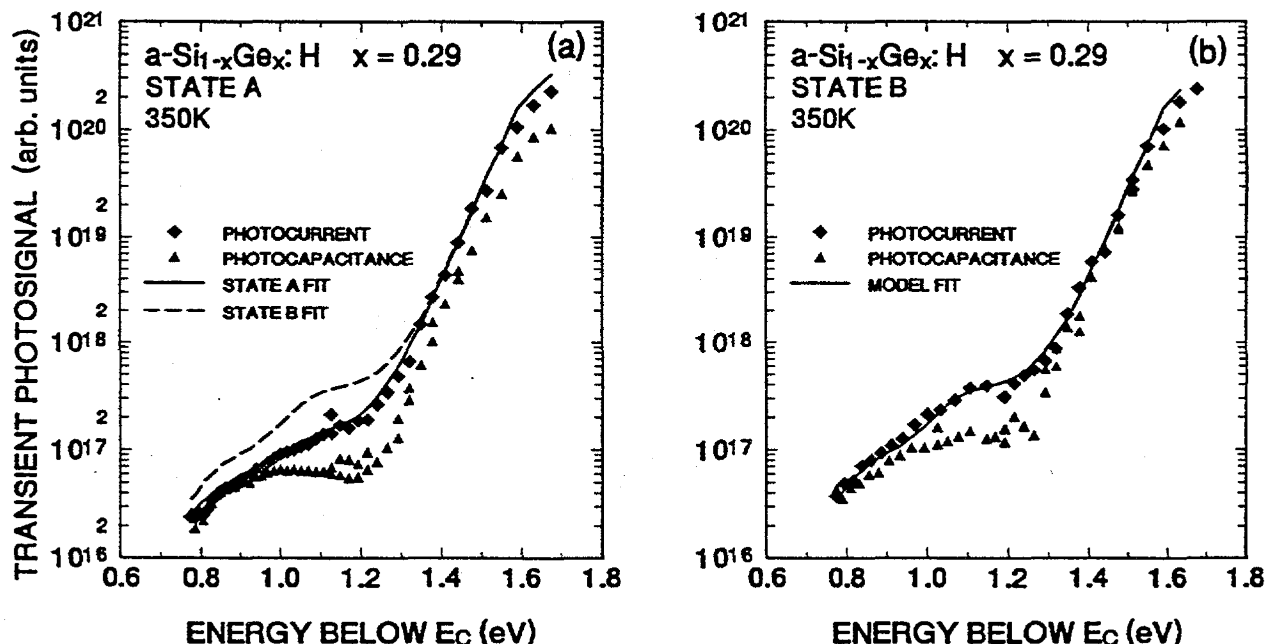

FIG. 11. (a). Transient photocurrent and photocapacitance spectra for the dark annealed state of an $x = 0.29$ a-$Si_{1-x}Ge_x$:H sample. The solid lines drawn through the photocurrent data represents the model fit to obtain the defect band transition energies. The dashed line is the state B photocurrent dependence and is drawn to show that the deep defect band has increased by roughly a factor of 3 after light soaking. (b) Transient photocurrent and photocapacitance spectra for the same sample (and same measurement temperature) after light soaking. The solid line is again a model fit. Note that the ratio of the photocurrent/photocapacitance spectra in the tail region has decreased markedly compared to the state A spectra.

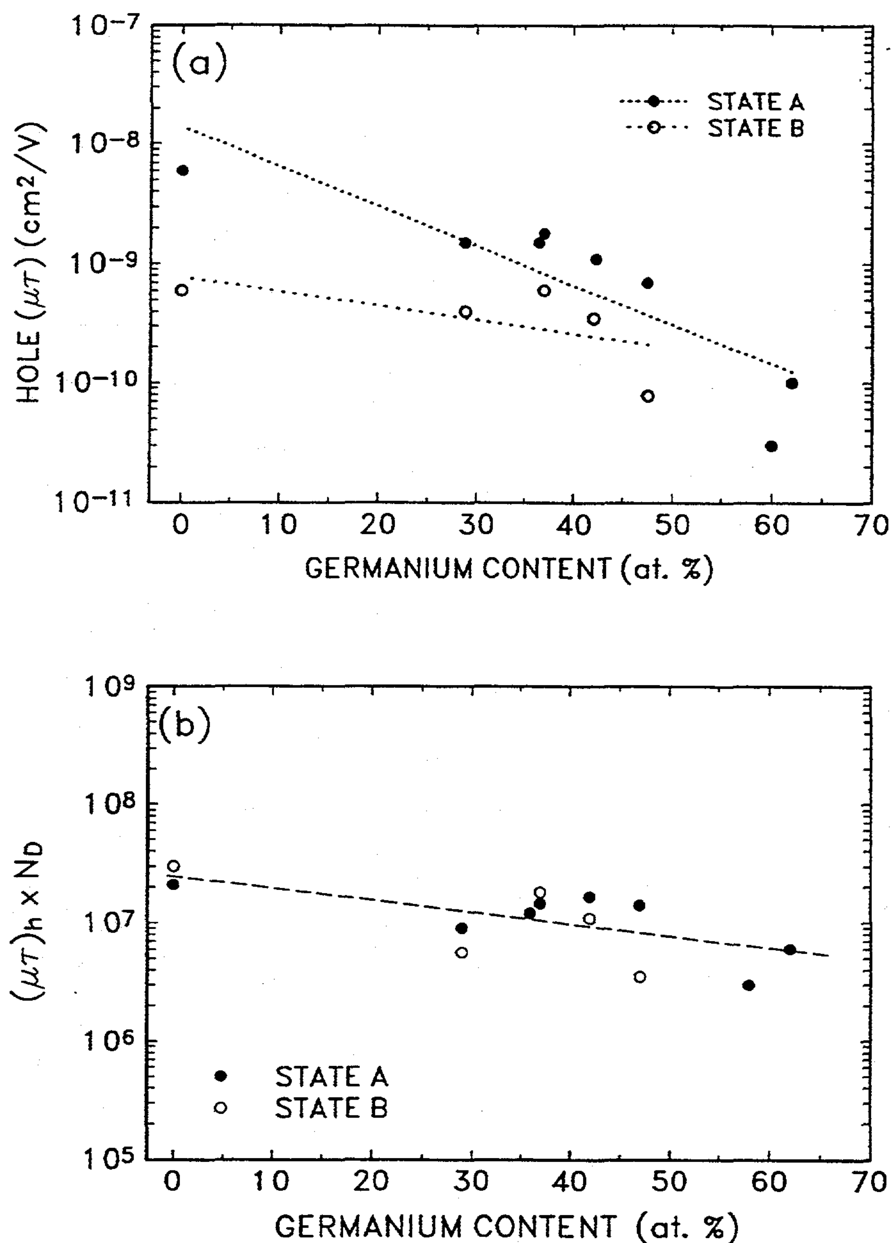

FIG. 12. (a). Hole $\mu\tau$ products *vs.* alloy composition before and after light soaking. (b). The same data but multiplied by the corresponding defect densities in each case. Note that these $(\mu\tau)_h N_D$ products are nearly independent of whether the samples are in states A or B. This indicates that both intrinsic and light-induced defects have very similar hole trapping properties.

7.0 SUMMARY AND CONCLUSIONS

In this report we have described the results of a fairly complete characterization of a series of a-$Si_{1-x}Ge_x$:H samples grown at the University of Delaware by the photo-CVD method. A summary of our results is given in Table I which lists the alloy compositions, optical gaps, Urbach energies, deep defect densities, and $\mu\tau$ products of holes for alloys within the composition range: $0.29 < x < 0.62$ $(1.3 < E_{opt} < 1.57)$. Results for 2 samples at the endpoints (x=0 and x=1) are also given. A few of our preliminary results are listed for sample properties after light degradation. However, possible conclusions from these must be tempered by the fact that different types and levels of light exposure were employed (as indicated) for each of the samples listed.

TABLE I. Summary of Properties Determined for Photo-CVD a-$Si_{1-x}Ge_x$:H Alloy Series. Note that the light induced changes were produced by different types of light exposure as has been noted.

Germanium Fraction, x	Optical Gap (eV)	Urbach Energy (meV)	St. A Defect Density (cm^{-3})	St. A $(\mu\tau)_h$ (cm^2/V)	St. B Defect Density (cm^{-3})	St. B $(\mu\tau)_h$ (cm^2/V)
0.00	1.68	48	3.5×10^{15}	6.0×10^{-9}	(a)5.0×10^{16}	6×10^{-10}
0.29	1.57	50	6.0×10^{15}	1.5×10^{-9}	(b)1.6×10^{16}	3.5×10^{-10}
0.37	1.51	51	8.0×10^{15}	1.8×10^{-9}	(b)3.0×10^{16}	6×10^{-10}
0.42	1.47	51	1.5×10^{16}	1.1×10^{-9}	(b)3.4×10^{16}	3.2×10^{-10}
0.47	1.40	52	2.0×10^{16}	7×10^{-10}	(c)4.4×10^{16}	8×10^{-11}
0.58	1.35	57	1.0×10^{17}	3×10^{-11}	---	---
0.62	1.30	55	6.0×10^{16}	1×10^{-10}	---	---
1.00	1.10	50	9×10^{17}	---	---	---

(a) Kr Laser, 4.5 W/cm^2, 1000s; (b) Filtered ELH Source, 200-400 mW/cm^2, >50h; (c) Ti Sapphire Laser, 4 W/cm^2, 3000s

Our most general conclusion is that these photo-CVD samples seem to represent what is close to the "state-of-the-art" in present a-Si,Ge:H alloys. That is, by comparing our results with corresponding values given in the literature, we find equal or superior properties in terms of bandtail widths and stable defect densities. This conclusion is consistent with a statement put forward in an earlier study of glow discharge a-Si,Ge:H; namely, that as the rf power level was decreased, the sample properties were observed to improve monotonically. [10] Thus the photo-CVD growth process may well represent the extremal limit of this previously observed trend. Our ongoing studies have just started examining several solar cell quality glow discharge a-Si,Ge:H films. Thus we hope to test this conclusion in more detail.

Our second main result is that we can assign defect energy levels from a detailed analysis of our transient sub-band-gap photocapacitance and photocurrent spectra. We find clear evidence for two distinct defect sub-bands, one at roughly midgap and the other in the upper half of the gap, above E_F. We also determined the energy dependence of these defect bands within the gap as the Ge alloy fraction, x, was varied. We found that the midgap defect level appeared to track the conduction band more closely than the valence band (for the shallow level our data was insufficient to decide whether it followed one band more closely). The shallow level was also found to exhibit a suppression of its thermal release of trapped electrons. This suggests a large degree of defect relaxation, as has been discussed previously [5,6].

Finally, we have found that the trapping lifetime related $\mu\tau$ products for holes decrease in direct proportion to the density of midgap defects in these samples. This appears to be the case regardless of whether we are dealing with stable defects or defects created by light soaking. However, at Ge composition fractions exceeding 50at.% there appears to be an additional decrease in $(\mu\tau)_h$ on top of this. We tentatively attribute this to a larger proportion of charged defects in such samples.

For future study on the low gap alloys, we plan to add some additional photo-CVD samples to the series studied so far, particularly in the lower and higher alloy range. We also plan to employ more detailed ESR and photoconductivity measurements to try to elucidate the unusual electron trapping properties suggested in our studies thus far. And we plan to obtain a-Si,Ge:H alloy samples grown by a variety of other methods (conventional and remote rf discharge, hot-wire, etc.) to determine whether the current baseline of properties established by the photo-CVD samples really represents any kind of optimum limit.

8.0 REFERENCES

1. D.E. Albright, N. Saxena, C.M. Fortmann, R.E. Rocheleau, T.W.F. Russell, AIChE Journal 36, 1555 (1990).

2. C.E. Michelson, A.V. Gelatos, and J.D. Cohen, Appl. Phys. Lett. 47, 412 (1985).

3. K.K. Mahavadi, K. Zellama, J.D. Cohen, and J.P. Harbison, Phys. Rev. B35, 7776 (1987).

4. J.D. Cohen and A.V. Gelatos, in *Advances in Disordered Semiconductors Vol I: Amorphous Silicon and Related Materials*, ed. by H. Fritzsche (World Scientific, Singapore, 1988), pp. 475-512.

5. J. David Cohen, Thomas Unold, A.V. Gelatos, and C.M. Fortmann, J. Non-Cryst. Solids 141, 142 (1992).

6. T. Unold, J.D. Cohen, and C.M. Fortmann, Mat. Res. Soc. Symp. Proc. 258, 499 (1992).

7. J. Hautala and J.D. Cohen, Mat. Res. Soc. Symp. Proc., in press.

8. T. Unold, Ph.D. Thesis, University of Oregon, 1993 (unpublished).

9. S. Aljishi, Z E. Smith, and S. Wagner, in *Advances in Disordered Semiconductors Vol I: Amorphous Silicon and Related Materials*, ed. by H. Fritzsche (World Scientific, Singapore, 1988), pp. 887-938.

10. M. Stutzmann, R.A. Street, C.C. Tsai, J.B. Boyce, and S.E. Ready, J. Appl. Phys. 66, 569 (1989).

11. A.V. Gelatos, K.K. Mahavadi, J.D. Cohen, and J.P. Harbison, Appl. Phys. Lett. 53, 403 (1988).

12. L. Chen, J. Tauc, J.-K. Lee, and E.A. Schiff, Phys. Rev. B43, 11694 (1991).

13. Fortmann, C.M., Albright, D.E, Campbell, I.H., and Fauchet, P.M., Mat. Res. Soc. Symp. Proc. 164, 315 (1990).

14. B. von Roedern, Appl. Phys. Lett. 62, 1369 (1993).

15. Note: This expression is in a slightly corrected form from what had appeared in Refs. 4, 5, and 6.

Document Control Page	1. NREL Report No.	2. NTIS Accession No.	3. Recipient's Accession No.
	NREL/TP-451-5737	DE93018205	

4. Title and Subtitle
Microscopic Origins of Metastable Effects in a-Si:H and Deep Defect Characterization in a-Si,Ge:H Alloys

5. Publication Date
August 1993

6.

7. Author(s)
J. David Cohen

8. Performing Organization Rept. No.

9. Performing Organization Name and Address
University of Oregon
Eugene, Oregon

10. Project/Task/Work Unit No.
PV341101

11. Contract (C) or Grant (G) No.
(C) XG-1-10063-1
(G)

12. Sponsoring Organization Name and Address
National Renewable Energy Laboratory
1617 Cole Blvd.
Golden, CO 80401-3393

13. Type of Report & Period Covered
Technical Report
1 February 1992 - 31 January 1993

14.

15. Supplementary Notes
NREL technical monitor: B. von Roedern

16. Abstract (Limit: 200 words)
This report describes work under Phase II of a subcontract to evaluate low-mobility-gap a-Si,Ge:H alloy films. The results are based primarily on a variety of junction capacitance techniques: admittance spectroscopy, transient photocapacitance (and photocurrent), and drive-level capacitance profiling. A series of eight a-Si,Ge:H alloy samples grown by photo-chemical vapor deposition (photo-CVD) at the Institute of Energy Conversion, University of Delaware encompassed the range of optical gaps from 1.3 to 1.6 eV, and corresponding Ge fractions from about 20 at% to 60 at%. We employed a variety of junction capacitance techniques to determine deep defect energies and densities, Urbach band-tail energies, and $\mu\tau$ products for holes. Electron microprobe analysis provided fairly accurate Ge fractions for our samples, thus enabling us to establish clear trends in the measured electronic properties as a function of the Ge fraction. We concluded that these photo-CVD samples exhibited equal or superior properties in terms of band-tail widths, and stable defect densities compared to any reported results on a-Si,Ge:H samples grown by glow discharge. By assigning defect energy levels from a detailed analysis of our transient sub-band-gap photocapacitance and photocurrent spectra, we found clear evidence for two distinct defect subbands, one at roughly midgap and the other in the upper half of the gap. The trapping lifetime related $\mu\tau$ products for holes decreased in direct proportion to the density of mid-gap defects in these samples. This appears to be the case regardless of whether we are dealing with stable defects or defects created by light-soaking.

17. Document Analysis

a. Descriptors
amorphous silicon ; germanium ; characterization ; alloys ; photovoltaics ; solar cells

b. Identifiers/Open-Ended Terms

c. UC Categories
271

18. Availability Statement
National Technical Information Service
U.S. Department of Commerce
5285 Port Royal Road
Springfield, VA 22161

19. No. of Pages
29

20. Price
A03

Form No. 0069E (6-30-87)